Evaluation of a New Experimental Geometry for ultra-fast Time Resolved Diffraction Experiments using a Laser-Produced Plasma Source

Experimental Set-up and Image Processing

Master's thesis
by
Eva Danielsson

Lund Reports on Atomic Physics, LRAP-309
Lund, August 2003

Abstract

This diploma work evaluates a new set-up for ultra-fast time-resolved x-ray diffraction experiments. The geometry is supposed to be less sensitive for pulse-to-pulse fluctuations in pump-probe experiments. A laser-produced plasma was used as x-ray source and a CCD camera as detector. Photon counting was applied to measure the results. To achieve useable pictures, good image processing is required and a special algorithm was written for this purpose in Matlab. The goal was to see a static Laue pattern from thin crystals and to perform the image processing.

Several difficulties with the experimental set-up were discovered. In the first place the handling of the sample proved to be a problem. Bragg reflection was detected but no Laue pattern.

The image processing was successful, though. An algorithm for pixel summation was written and it gave satisfactory result. More photons were counted especially when the pictures were more sparsely populated. Also the results of only showing a specific energy interval in the image proved to be useful.

Sammanfattning

I detta examensarbete utvärderas en ny typ av uppställning för ultrasnabba tidsupplösta diffraktionsexperiment. Geometrin förmodas vara mindre känslig för puls-till-puls-fluktuationer i pump-probexperiment. Ett laserproducerat plasma användes som röntgenkälla och en CCD-kamera som detektor. Fotonräkning tillämpades för att mäta resultaten. För att få användbara bilder krävs en god bildbehandling av experimentella data och en särskild algoritm skrevs för detta syfte i Matlab. Målet var att i första hand se ett statiskt Lauemönster i transmissionsgeometri från tunna kristaller samt att genomföra bildbehandlingen.

Flera svårigheter med den experimentella uppställningen upptäcktes. Framförallt hanteringen av provet visade sig innebära problem. Braggreflektion kunde registreras men inte Lauemönster.

Bildbehandlingen gav mer framgång. En algoritm för pixelsummering skrevs och den gav tillfredsställande resultat. Fler fotoner kunde räknas om de detekterade signalerna inte låg alltför tätt i bilden. Även resultatet av att endast ta med ett visst energiintervall i bilden visade sig vara användbart.

Contents

1 Introduction 4
1.1 Time resolved x-ray diffraction studies 4
1.2 The aim of the project 6

2 Theory section 7
2.1 Crystals 7
2.1.1 Crystal lattice 7
2.1.2 Crystal structures 8
2.1.3 Reciprocal lattice 8
2.1.4 Crystal planes 9
2.2 X-ray diffraction 10
2.2.1 Principles 10
2.2.2 The Bragg law 10
2.2.3 Laue formulation 11
2.2.4 Allowed and forbidden reflections 14
2.2.5 Determining the Bragg angle 15
2.3 X-ray generation from laser-produced plasmas 15

3 The diffraction experiment 17
3.1 Basic principles 17
3.2 Set-up for x-ray generation 17
3.3 The CCD camera 19
3.3.1 The chip 19
3.3.2 Environment 19
3.3.3 Principles 20
3.3.4 Background 21
3.3.5 Photon counting 21
3.4 Optimising the lens 22
3.4.1 Set-up 22
3.4.2 Result of lens optimisation 23
3.5 Sample set-up 24
3.5.1 Diffraction results 26
3.6 Experimental problems 26
3.6.1 Additional attempts 27

4 Image processing 28
4.1 Background subtraction 29
4.2 Summation of adjacent pixel events 29
4.2.1 Result of pixel event summation 31
4.3 Energy selection 34

5 Summary 36
5.1 Part one: Experimental set-up 36
5.2 Part two: Image processing 36

6 Acknowledgements **38**

7 Bibliography **39**

Appendix **41**

1 Introduction

To study materials on the atomic scale, x-ray diffraction is an excellent tool. X-ray wavelengths are small enough to resolve the interatomic distances and the method is very reliable. The method is non-destructive and can be used for identification and quantiative measurements of crystalline solids. Father and son Bragg discovered the method in 1913 and ever since its discovery, x-ray diffraction has been widely used in a number of scientific fields such as crystallography, mineralogy, biochemistry, and material science.

In nature, there are many processes that take place very rapidly, faster than a few pico-seconds. Topics that may be interesting for further studies are disordering of atoms, forming of molecules and structure dynamics - fundamental events in biology, chemistry and physics. However, picosecond is a time interval that is far too short for the human eye to observe so we need some aid to register the temporal development of these processes. The time resolved x-ray diffraction is a method that has been developing during the last decade and the aim is to achieve higher time resolution to be able to study the ultra-fast processes mentioned above.

1.1 Time resolved x-ray diffraction studies

Many of these ultra-fast events take place only when triggered by some external input, e.g. illuminated by a light pulse. The usual way to observe the time development of these events is to construct a *pump-probe* experiment. The sample is pumped with a *pump* beam, e.g. a laser pulse that photo-triggers the sample. Then the following *probe* does a 'read-out', e.g. a x-ray pulse that gives a diffraction pattern.

The pump-probe set-up can be performed according to two different principles: using a fast detector and a long probe pulse, or with a short probe and a slow detector, see *figure 1.1*. There are benefits and drawbacks for both kinds. A fast detector and a long probe make it possible to detect the entire reaction in just one experiment [1]. The detector resolves the event in time steps while the sample is continuously probed. However, the sensitivity of the detector decreases with higher time resolution. With a short probe a slow, but sensitive, detector can be used. The experiment then has to be repeated a number of times with different delay time between the pump and the probe to completely cover every time step of the event [2, 3].

To achieve short x-ray pulses one can use either *synchrotron radiation* or *laser-produced plasmas* as sources. The synchrotron radiation has a higher repetition rate but longer pulses (~100 ps) compared to the plasma source (~100 fs). The synchrotron source is thus considered a 'long' probe, which need to be detected by a fast detector, e.g. a streak camera [4]. The streak camera can resolve events down to < 1.6 ps [5].

When performing the experiments one has to distinguish between reversible and irreversible processes. If the experiment is repeated with different time delays the process must be reversible, since the conditions must be identical for every time delay. Hence, the synchrotron pulse can be used in single shot experiments where the sample is destroyed by the pump pulse. The plasma pulse has to be repeated and the sample must then return to the initial state after some time after the probe pulse.

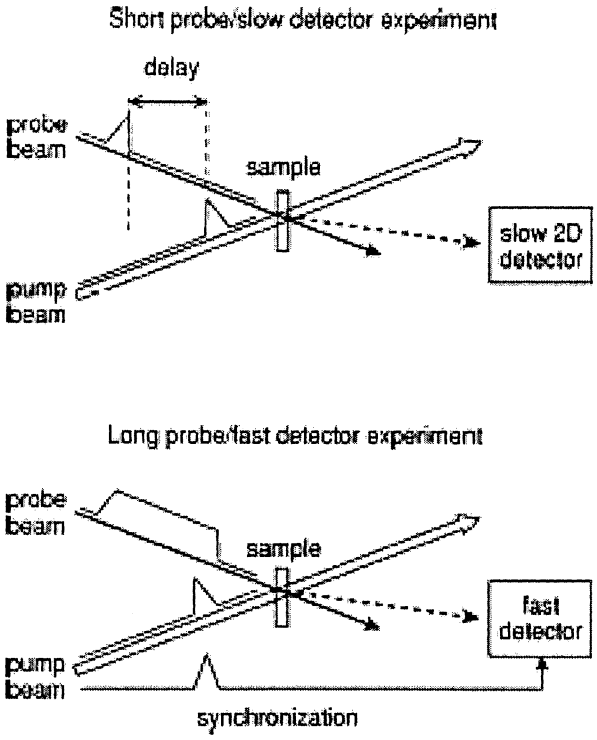

Figure 1.1. Two types of pump-probe experiments [4].

Synchrotron x-ray pulses have been utilised in experiments investigating e.g. penetration depth of pulse damage [6], biochemical photolysis [2], structural dynamics [7], phase transitions [1, 8] and diffraction of phonons [9].

The laser produced plasma x-ray source gives pulses that are assumed to be of the same length as the plasma producing laser pulse [10-12]. These x-ray pulses are considered short; they are of the same order as molecular vibrations, i.e. $\sim 10^{-15}$ s. The plasma source has made it possible to detect e.g. non-thermal melting in semiconductors in real time [12]. This process could clearly be distinguished from the slower thermal melting, which take several picoseconds to occur. Other experiments have showed ultra-fast structure dynamics in crystals [13].

1.2 The aim of the project

To study structures of solids several diffraction spots are needed to interpret the result properly. This can be achieved by choosing the correct experimental set-up: The two most common geometries for diffraction experiment are the *Bragg* geometry and the *Laue* geometry. In the Bragg case, a monochromatic and collimated beam is incident on a moving crystal. When the crystal oscillates different Bragg angles are achieved and several reflections can be detected. For the Laue case the crystal is stationary and the beam is polychromatic. The reflection angles vary for different wavelengths; hence, this method also gives multiple reflections. A new idea, considered in this project, is to use a monochromatic, but divergent beam in Laue geometry to detect multiple reflections. A specific set-up for this condition was evaluated in the diploma work.

One of the main issues in improving the time-resolved experiments is to shorten the accumulation time. The long synchrotron pulse can give sufficient radiation in only one shot, but for higher time resolution shorter probe pulses are needed. The shorter plasma femtosecond pulse is much weaker and has to be repeated and the diffraction signals accumulated over several pulses. The background from the plasma source is considerably higher than from the synchrotron and the signal noise in a slow detector will also increase with time and the resulting images have to be processed in a way that reduces the noise but keeps the diffraction signal. This was the second of the two purposes with this diploma work; to write an algorithm that processes images for further photon counting.

2 Theory section

Three different topics will be treated here: general crystal theory, x-ray diffraction and x-ray generation from plasmas. These subjects are considered sufficient for understanding the main part of this work.

2.1 Crystals

2.1.1 Crystal lattice

In solids that are crystalline atoms are ordered in a periodic *lattice* throughout the crystal. The *Bravais lattice* is a concept used to describe the array of atoms, or any other corresponding units such as ions or molecules, which periodically build up the crystal. The Bravais lattice has the property of looking the same irrespective of from which point of the lattice it is viewed. The primitive vectors $\mathbf{a}_1$, $\mathbf{a}_2$, and $\mathbf{a}_3$, three arbitrary, but linearly independent, vectors generate it. The positions of the units in the lattice can be described by a linear combination: $\mathbf{R} = n_1\mathbf{a}_1 + n_2\mathbf{a}_2 + n_3\mathbf{a}_3$, where n_i is an integer. The length of the primitive vectors is thus the distance between two adjacent array points. The distance is called the *lattice constant*. In a cubic lattice the three vectors are of course of the same length but for other crystal systems there are more than one lattice constant and one must also specify the angles between the axes. This length is an important property of the crystal, and is easily found in tables over physical constants.

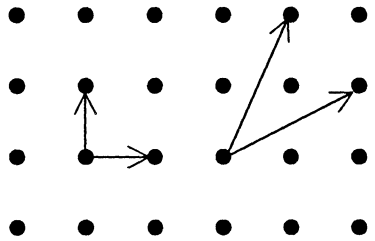

Figure 2.1. 2-dimensional Bravais lattice, with two different sets of primitive vectors.

A volume of the lattice that contains only *one* lattice point and can be translated along all vectors without creating overlap or empty space is called a *primitive cell*. Just as the primitive vectors they can be chosen in several different ways.

This Bravais depiction can be a little misleading, though. The symmetry of the Bravais lattice might be concealed, as in *figure 2.2*. To avoid this one usually uses the concept of *conventional unit cell*. It is a cell that possesses the proper symmetry and it can also be repeated like the primitive cell but through another set of basis than the primitive vectors.

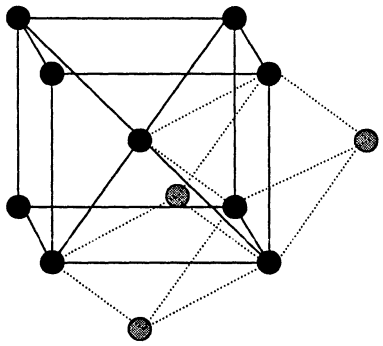

Figure 2.2 Primitive Bravais cell (dotted line) and conventional unit cell (solid line) for the body centred cubic lattice.

2.1.2 Crystal structures

The conventional unit cell is chosen so that the symmetry becomes clear and thus it doesn't have to be primitive, i.e. it can contain more than one atom. Two important structures: body centred cubic, *bcc* (*figure 2.2.*), and face centred cubic, *fcc,* contains, respectively, 2 and 4 atoms. The term *crystal structure* is used when speaking of the physical crystal instead of the more abstract idea of Bravais lattices.

2.1.3 Reciprocal lattice

For further exploration of the crystal world we need to define the *reciprocal space*. This is a powerful tool for understanding most periodic systems.

Let **R** be a set of lattice vectors that span a Bravais lattice. A plane wave $e^{i\mathbf{k}\cdot\mathbf{r}}$ will have the periodicity of the lattice only for certain wave vectors **k**. This set of wave vectors, **K**, generates the reciprocal lattice. For any vector **r** in real space these relations must then be fulfilled:

$$e^{i\mathbf{k}\cdot(\mathbf{r}+\mathbf{R})} = e^{i\mathbf{k}\cdot\mathbf{r}} \Rightarrow e^{i\mathbf{K}\cdot\mathbf{R}} = 1$$

The reciprocal primitive vectors, $\mathbf{b}_i$, are constructed from the real primitive vectors, $\mathbf{a}_i$:

$$\mathbf{b}_1 = 2\pi \frac{\mathbf{a}_2 \times \mathbf{a}_3}{\mathbf{a}_1 \cdot (\mathbf{a}_2 \times \mathbf{a}_3)}$$

$$\mathbf{b}_2 = 2\pi \frac{\mathbf{a}_3 \times \mathbf{a}_1}{\mathbf{a}_2 \cdot (\mathbf{a}_3 \times \mathbf{a}_1)}$$

$$\mathbf{b}_3 = 2\pi \frac{\mathbf{a}_1 \times \mathbf{a}_2}{\mathbf{a}_3 \cdot (\mathbf{a}_1 \times \mathbf{a}_2)}$$

The reciprocal vectors are orthogonal to two of the real lattice vectors and:

$$\mathbf{b}_i \cdot \mathbf{a}_j = 2\pi\delta_{ij}$$

$$\delta_{ij} = \begin{cases} 1 & i = j \\ 0 & i \neq j \end{cases}$$

The real vectors were constructed:

$$\mathbf{R} = n_1\mathbf{a}_1 + n_2\mathbf{a}_2 + n_3\mathbf{a}_3$$

where the n_i are integers. In the same way the reciprocal lattice vectors are constructed:

$$\mathbf{k} = k_1\mathbf{b}_1 + k_2\mathbf{b}_2 + k_3\mathbf{b}_3$$

From the equations above follows the scalar product $\mathbf{k}\cdot\mathbf{R} = 2\pi\,(k_1n_1 + k_2n_2 + k_3n_3)$. To fulfil the condition $e^{i\mathbf{k}\cdot\mathbf{R}} = 1$ for any value of n_i it is obvious that the coefficients in the reciprocal vector, k_i, must also be integers.

2.1.4 Crystal planes

A *crystal plane* contains at least three non-collinear lattice points. The orientation of a plane is defined by the normal, which can be described by the reciprocal vectors $\mathbf{b}_1\mathbf{b}_2\mathbf{b}_3$ with the so-called *Miller indices* (integers) as coefficients:

$$\mathbf{H}_{hkl} = h\mathbf{b}_1 + k\mathbf{b}_2 + l\mathbf{b}_3$$

The length of the vector $\mathbf{H}$ is the reciprocal of the distance d between two adjacent and parallel planes:

$$|\,\mathbf{H}_{hkl}\,| = 2\pi/d$$

Consider two adjacent and parallel planes, one of which passes through the origin. The other will then intercept the lattice axes at $\mathbf{a}_1/2\pi h$, $\mathbf{a}_2/2\pi k$ and $\mathbf{a}_3/2\pi l$. The planes are commonly referred to as *hkl* planes. Crystal planes in cubic structures are often written with just the Miller indices enclosed in parentheses (*hkl*). The notation {100} are equivalent to all three planes (100), (010) and (001). To include the negative directions (-100), (0-10) and (00-1), the notation is ⟨100⟩.

2.2 X-ray diffraction

To examine crystal structures by optical methods the wavelengths have to be shorter than the inter-atomic distances in the lattice. X-rays are short enough and also have the benefit of being fairly easy to generate and they don't damage the sample while probing it. The x-ray diffraction method is a useful and well-known method. W. H. and W.L. Bragg, father and son, discovered the phenomenon in the year 1913. This theory and method has been widely used by crystallographers ever since the discovery. The periodic structures of crystals can easily be revealed by this method.

2.2.1 Principles

The Braggs noticed that crystalline solids gave a specific reflection pattern when illuminated by x-rays. The idea of crystal planes that could scatter the x-rays elastically helped out to make a proper interpretation:

The principle of x-ray diffraction is that x-ray photons are incident onto a crystal and scatter elastically onto the atoms. The photons are assumed to scatter specularly, i.e. the incident angle equals the reflection angle. The reflections from successive crystal planes will interfere constructively if the path difference is a multiple of the wavelength.

2.2.2 The Bragg law

For each wavelength there are corresponding angles of incidence that will cause intense reflection peaks, *Bragg peaks*. The required condition for the peaks to appear is known as the *Bragg law*. The distance between two adjacent crystal planes is denoted d and the incident angle is θ_B, also called the Bragg angle. The Bragg law is written:

$$n\lambda = 2d_{hkl} \sin\theta_B$$

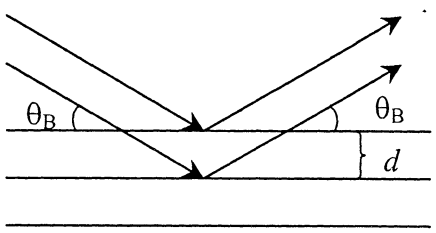

Figure 2.3. The Bragg reflection schematically for the incident angle θ_B *and the inter-planar distance* d. *The path difference between the two beams is* $2d \sin\theta_B$.

Vector formulation of the Bragg law

The Bragg law can also be expressed in vector form by the incident and diffracted beams. The unit vectors for these beams are called $\mathbf{s}_0$ and $\mathbf{s}$. The wave vectors are expressed by multiplying the unit vectors with the inverse wavelength λ^{-1}. The difference between the two wave vectors is perpendicular to the plane, since they are assumed to make the same angle to the plane. The resultant is the reciprocal vector $\mathbf{H}$, with a length of the inverse distance between the planes:

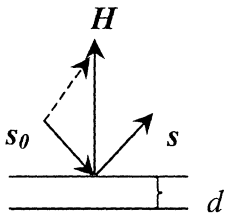

$$\frac{s - s_0}{\lambda} = H_{hkl} = \frac{1}{d}$$

Figure 2.4. Vector formulation of Bragg diffraction.

2.2.3 Laue formulation

The Laue formulation of x-ray diffraction is derived without these assumptions of mirror reflectance. Consider the scattered x-ray beam at point P at a distance R from the crystal origin. The nth atom in the crystal is represented by the position vector $\mathbf{R}_n = m_1\mathbf{a}_1 + m_2\mathbf{a}_2 + m_3\mathbf{a}_3$

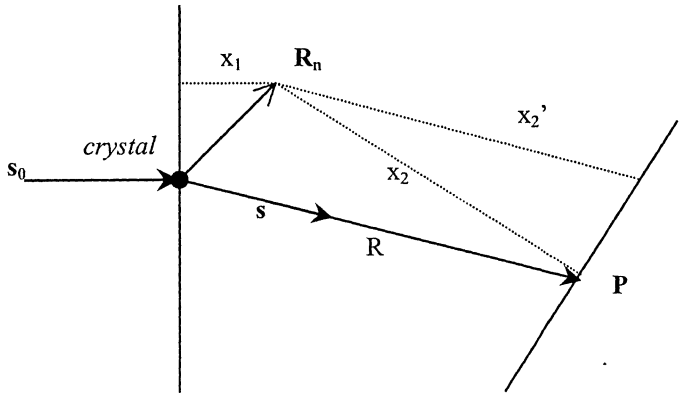

Figure 2.5. Scattering by a crystal. The observer is placed in P *and the atom* n *is positioned at* $\mathbf{R}_n$. *The incident and the diffracted beams are represented respectively by unit vectors* $\mathbf{s}_0$ *and* $\mathbf{s}$. *The length of* $\mathbf{R}_n$ *is exaggerated.*

The amplitude ε_P of the electric field in P due to the scattering from the nth atom can be written as:

$$\varepsilon_P = \frac{E_0 e^2}{mc^2 x_2} f_n e^{i\left[2\pi\nu t - \frac{2\pi}{\lambda}(x_1 + x_2)\right]}$$

where E_0 is the amplitude of the primary beam, e and m are the charge and mass of the electron. The letters ν and λ are, respectively, the frequency and the wavelength. The atomic scattering factor f will be explained later.

We apply the plane wave approximation, since the distance between the source and the observer is much larger than the distance between the atom and the crystal origin. The plane wave travels a total distance of $(x_1 + x_2)$ from the crystal to the observer P and it can thus be approximated to $(x_1 + x_2')$. The distance can also be expressed by (*cf. figure 2.5*):

$$\mathbf{R}_n \cdot \mathbf{s}_0 + \mathrm{R} - \mathbf{R}_n \cdot \mathbf{s} = \mathrm{R} - (\mathbf{s}-\mathbf{s}_0) \cdot (m_1\mathbf{a}_1 + m_2\mathbf{a}_2 + m_3\mathbf{a}_3)$$

The exponential form of the field in P is then:

$$\varepsilon_P = \frac{E_0 e^2}{mc^2 R} f_n e^{i\left[2\pi\nu t - \frac{2\pi}{\lambda}(R-(s-s_0)\cdot(m_1a_1+m_2a_2+m_3a_3)\right]}$$

The resultant field is calculated by summing over the n atoms and over all N unit cells.

Atomic scattering factor

The *atomic scattering factor* (f_n) is the amplitude of elastic scattering per atom expressed in electron units. The scattered beam from one *electron* can be written as:

$$\varepsilon_e = \frac{E_0 e^2}{mc^2 R} e^{2\pi i(\nu t - R/\lambda)} \sum_n e^{(2\pi i/\lambda)(s-s_0)\cdot r_n}$$

where R is the distance from the origin of the atom to the observer and $\mathbf{r}_n$ is the position of the electron n. The vector relations are the same as with the scattering by the small crystal (*cf. figure 2.5*).

The expression is valid providing the plane wave approximation is used and the phase jump of 180° is left out. Another simplification made here is that the electron is considered to be a point charge. If instead the electron is regarded as a charge density ρ in a specific volume element dV, the amplitude is expressed:

$$\varepsilon_e = \frac{E_0 e^2}{mc^2 R} e^{2\pi i(\nu t - R/\lambda)} \int e^{(2\pi i/\lambda)(s-s_0)\cdot r_n} \rho dV$$

The integral over the volume is called the *scattering factor* for the electron e. To determine the *atomic* scattering factor a summation of all electrons is made. The expression gets quite simple if the electron distribution is assumed to be *spherical symmetric*. The radial distribution of the charge is then the only quantity you need to know to determine the atomic scattering factor f_n. By setting

$$k = \frac{4\pi \sin\theta}{\lambda}$$

the atomic scattering factor, i.e. the amplitude of elastic scattering per electron, is:

$$f = \sum_n \int_0^\infty 4\pi r^2 \rho(r) \frac{\sin kr}{kr} dr$$

Structure factor

Returning to the small crystal once again, the resulting diffracted amplitude in point *P* is determined by summing over all *n* atoms in the crystal and over m_1 m_2 m_3 for all unit cells. The sum over *n* contains the position vectors for the atoms in the unit cell and is called the *structure factor, F*. This is an important term when determining the structure of the unit cell.

$$F = \sum_n f_n e^{(2\pi i/\lambda)(s-s_0)\cdot R_n}$$

The Laue equations

The crystal has the size $N_1a_1N_2a_2N_3a_3$, where *N* indicates the number of unit cells. The summations in all three directions over the unit cells get the form:

$$\sum_{m_i=0}^{N_i-1} e^{(2\pi i/\lambda)(s-s_0)\cdot m_i a_i} = \frac{e^{(2\pi i/\lambda)(s-s_0)\cdot N_i a_i} - 1}{e^{(2\pi i/\lambda)(s-s_0)\cdot a_i} - 1}$$

When multiplying the amplitude with its complex conjugate and a factor c/8π, we receive the intensity in *P*, i. e. the quantity that we can actually measure. The intensity in the three different lattice vector directions $\mathbf{a}_i$ is thus proportional to:

$$\left(\frac{e^{iN_ix_i} - 1}{e^{ix_i} - 1}\right)\left(\frac{e^{-iN_ix_i} - 1}{e^{-ix_i} - 1}\right) = \frac{2 - 2\cos N_i x_i}{2 - 2\cos x_i} = \frac{\sin^2 N_i x_i / 2}{\sin^2 x_i / 2}$$

where $x_i = (2\pi/\lambda)(\mathbf{s}\text{-}\mathbf{s}_0)\cdot\mathbf{a}_i$.

When $x/2 = n\pi$ and *n* is an integer, the expression $sin^2\ x/2 \rightarrow 0$. By expanding this expression we see that maximum is N^2. The amplitude is thus very large at this condition. Elsewhere the expression is aproximately zero.

$$x_i/2 = (\pi/\lambda)(\mathbf{s}\text{-}\mathbf{s}_0)\cdot\mathbf{a}_i = n\pi$$

The three *Laue equations* are written:

$$(\mathbf{s}\text{-}\mathbf{s}_0)\cdot\mathbf{a}_1 = n_1\lambda$$
$$(\mathbf{s}\text{-}\mathbf{s}_0)\cdot\mathbf{a}_2 = n_2\lambda$$
$$(\mathbf{s}\text{-}\mathbf{s}_0)\cdot\mathbf{a}_3 = n_3\lambda$$

To reach a total maximum intensity this condition must simultaneously be fulfilled for all three $\mathbf{a}_1\mathbf{a}_2\mathbf{a}_3$. The maximum intensity represents the Bragg peaks and from here it is easy to see the equivalence between Bragg and Laue formulation of the x-ray diffraction:

Consider a vector in reciprocal space: $\mathbf{k} = (n_1\mathbf{b}_1 + n_2\mathbf{b}_2 + n_3\mathbf{b}_3)$. The coefficients n_j can be determined by multiplying with $\mathbf{a}_1\mathbf{a}_2\mathbf{a}_3$. Hence, a way to notate the reciprocal vector is $\mathbf{k} = (\mathbf{k}\cdot\mathbf{a}_1)\mathbf{b}_1 + (\mathbf{k}\cdot\mathbf{a}_2)\mathbf{b}_2 + (\mathbf{k}\cdot\mathbf{a}_3)\mathbf{b}_3$. Using the Laue equations, where the reciprocal vector is called $(\mathbf{s}\text{-}\mathbf{s}_0)$, the result gets:

$$(\mathbf{s}\text{-}\mathbf{s}_0) = \lambda(n_1\mathbf{b}_1 + n_2\mathbf{b}_2 + n_3\mathbf{b}_3)$$

Let us call the integers $n_j = h$, k and l and the relation is clear:

$$(\mathbf{s}\text{-}\mathbf{s}_0) = \lambda\mathbf{H}_{hkl}$$

2.2.4 Allowed and forbidden reflections

The intensity of the scattered x-rays is proportional to the amplitude of the electric field and thus also to the structure factor F. From the above-derived Laue equations we see that

$$F = \sum_n f_n e^{2\pi i(H\cdot R_n)} = \sum_n f_n e^{2\pi i(hm_{n1}+km_{n2}+lm_{n3})}$$

where m_{ni} is the coordinates along the real vectors. The intensity of the Bragg peaks depends thus on the structure factor, or more exactly, the reciprocal vectors. Consider the body centred cubic Bravais lattice. It can be regarded as a simple cubic lattice with a *basis*, i.e. one atom placed in (0, 0, 0) and another in (½, ½, ½) in the real lattice $\mathbf{a}_1\mathbf{a}_2\mathbf{a}_3$. The reciprocal lattice for this structure is also a simple cubic lattice, with the primitive vectors of length *(1/a)*. For simplicity, assume that *f* is equal to unity, and the structure factor then becomes:

$$F = 1 + e^{i\pi(h+k+l)} = 1 + (-1)^{(h+k+l)} = \begin{cases} 2 & h+k+l = even \\ 0 & h+k+l = odd \end{cases}$$

This means that there will only be a Bragg reflection (*allowed*) where the Miller indices make an even sum, and no reflection (*forbidden*) at all if the sum is odd.

Diffraction conditions for silicon

In this project Si crystals were used in the diffraction experiment. Silicon has *diamond structure*, which is not a Bravais lattice by definition. It can be considered as a *fcc* Bravais lattice with a two-point basis; atoms positioned at (0, 0, 0) and (¼, ¼, ¼). Putting this into the structure factor the result is:

$$F = 1 + e^{\frac{1}{2}i\pi(h+k+l)} = \begin{cases} 2 & h+k+l = 4n \\ 1 \pm i & h+k+l = odd \\ 0 & h+k+l = 4n+2 \end{cases}$$

Thus there are only Bragg peaks diffracted from planes where $(h + k + l)$ is a multiple of 4 or where all three indices are odd. If the sum of the indices is twice an odd number $(4n + 2)$ no reflection will appear.

2.2.5 Determining the Bragg angle

The lattice constants of a crystal are commonly denoted *a, b,* and *c,* and the angles between them are, respectively, α, β, and γ. These parameters are necessary for calculating the distance d_{hkl} between the planes *(hkl)*. The formula for this can be quite complicated, depending on the relative angles. The diamond structure is a *cubic* lattice in which the constants are $a = b = c$ and $\alpha = \beta = \gamma = 90°$. This makes the expression for the distance between planes in a cubic lattice very simple:

$$\frac{1}{d_{hkl}^2} = \frac{h^2 + k^2 + l^2}{a^2}$$

where a is the lattice constant. Combining this equation with the Bragg law gives:

$$\sin\theta_B = \frac{\lambda}{2a}\sqrt{\left(h^2 + k^2 + l^2\right)}$$

By e.g. detecting diffraction peaks from a certain wavelength and determine the reflection angle, one can thus get the lattice constant.

2.3 X-ray generation from laser-produced plasmas

A plasma consists mainly of free ions and charges and originates from gases, liquids or solids that have been almost completely ionised. The free electrons are hot, move fast and are able to penetrate into the cooler, surrounding and non-plasmatic material and ionise its atoms. These emitted electrons give rise to x-ray radiation, consisting of both a Brehmsstrahlung continuum and characteristic lines from the exposed target material. The continous radiation is due to deceleration of the fast electrons when they collide with nuclei, followed by emission of a photon. The continuum is assumed to scale as the Boltzmann distribution *exp(-E/kT)* [14]. The characteristic radiation originates when the fast electrons collide inelastically with inner electrons in the target. The inner electrons are emitted and the ionised atom deexcites and emits an x-ray photon.

To achieve plasma a high intensive laser beam can be focused onto e.g. most commonly; a solid metal target (foils, plates [11] or wires [15]), but also onto van der Waals clusters of noble gases [16]. The laser intensity for x-ray generation is typically 10^{15}-10^{17} W/cm^2 [5, 10, 16, 17]. To avoid distortion of the laser focus due to its passage through air, the plasma is created in a vacuum chamber. The size of the source, i.e. the focal spot is about 10-50 μm [4, 15]. This should be compared to a standard x-ray tube with a source size of 300-

1200 μm. One of the benefits of using the plasma x-ray source is the small size; it makes the experimental set-up more flexibel.

The main characteristic of the plasma x-ray source is the monochromatic and divergent beam. These features make it an interesting alternative for time-resolved diffraction experiments with Laue geometry; different directions would hit the sample and reflections from several crystal planes would be detected simultaneously. With the short probe pulse a slow, but sensitive, detector could be used. This was one of the main topic of this diploma work and since the start of the project similar experiments also have been published [15].

The pulse length of the plasma x-ray source is assumed to be of the same order as the laser pulse [10-12]. The hot and fast electrons from the plasma are only present during the laser pulse and the x-rays can only be generated while the plasma exists. The x-ray pulse lengths can thus be varied from ~100 fs to ~100 ns.

Another positive feature is that synchronisation with a pump beam easily can be done. A pump-probe experiment can be performed by using the plasma-producing laser as the pump laser.

Atomic number

The generation is dependent not only on the intensity of the laser pulse, it is also dependent on the atomic number of the target material. The higher the atomic number *Z,* the smaller the x-ray generation [10, 17, 18]. This means that it is easier to achieve soft x-rays, (0.5 –10 keV), than harder radiation (>10 keV), since the characteristic radiation depends on the binding energies of the inner electrons in the elements. Heavier atoms have larger binding energies, and thus the emitted photons have higher energies.

Prepulses

One way to further improve the generation is to use prepulses from the laser [10, 11 17, 19]. The prepulses are made to appear a few nanoseconds before the main pulse and they are approximately four orders weaker than the main pulse. These prepulses create a pre-plasma and the electron density gradient of the plasma changes and the absorption of fast electrons can be optimised [4].

Target

The emission from the target is dependent on position and structure [11]. If the laser energy is deposited deep inside the target, the x-ray photons are reabsorbed. The laser beam is not supposed to penetrate too deep into the material, but since a plasma is formed the laser creates a hole in the surface. In the experimental set-up, a mobile target solves this problem. The laser pulse will always hit a fresh surface, because the target is continuously moving.

3 The diffraction experiment

3.1 Basic principles

One of the two intentions with this project was to develop a new experimental geometry for time-resolved x-ray diffraction with a laser produced plasma as x-ray source (*see section 2.3)*. The aim was to observe a stationary Laue pattern from a 10 μm Si crystal and to evaluate the method for further pump-probe experiments.

The laser produced plasma has several benefits as x-ray source for time resolved diffraction experiments. It is assumed that the plasma provides x-ray pulses with a duration of the same order as the plasma producing pulse. This means that the x-ray pulses in this experiment was of the order 35 fs, since that is the present pulse length of the utilised TW laser.

The source can be synchronised with the pump beam, which conveniently can be linked from the very same laser beam that produces the plasma. The source is small, compared to traditional sources like the x-ray tube, and the experimental set-up can be made compact.

3.2 Set-up for x-ray generation

To generate characteristic x-ray radiation the laser produced plasma source was used. A high intensive laser pulse was focused onto a thin metal foil and the deposited energy transformed the metal into a plasma state. The radiation originate from free electrons in the plasma hitting surronding cold metal and ejecting inner electrons (*see section 2.3)*. The radiation used in the experiments was mainly the characteristic emission from copper ($Z = 29$, $K_\alpha = 8.0\ keV$). The Cu foil was 50 μm thin. Some evaluation of molybdenum ($Z = 42$, $K_\alpha = 17.4\ keV$) was also made.

The x-ray generation requires a vacuum environment in order to avoid distortion of the laser beam by non-linear interactions with air. There are several processes that could cause a breakdown such as phase modulation and changes in the refraction index in air. The experimental chamber was thus evacuated. The outer dimensions of the chamber was $40\times50\times24\ cm^3$. The outgoing window was made of 200 μm thin plastics which does not affect the intensity of the x-ray too much. To protect the scientist from unhealthy radiation the chamber was covered by lead blocks, which is a good absorber of x-rays.

As focusing element a planar-convex lens was used. The diameter was 47 mm and the focal length was 300 mm. The lens was placed inside the chamber on a motor-driven translational stage, for small adjustments of the focal position. The adjustment was controlled by manually operating the motor outside the chamber.

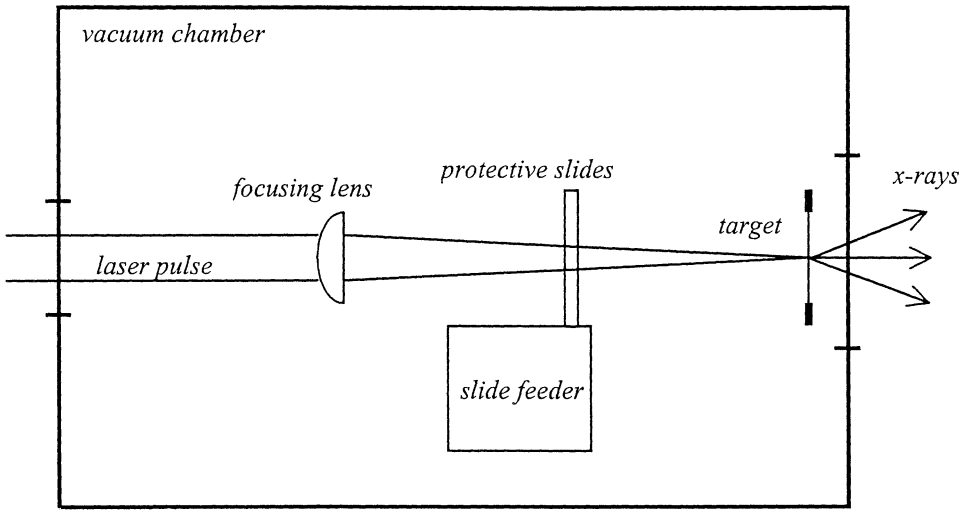

Figure 3.1. The experimental set-up for x-ray generating.

The target holder was moved by translation stages in horisontal and vertical direction, both controlled by a computer program. The holder was continously moving during experiments and this made it possible to always shoot at a fresh surface on the foil. The x-ray emission could temporarily be increased by shooting at the same spot [11], but the high intensity laser quickly burns a hole through the thin foil and therfore it was avoided.

To protect the optics from sputtered debris from the target a glass slide (100 μm) was placed between the target and the lens. The particles deposit on the slides and will not harm the lens. The laser intensity is almost unaffected if the slides are regularly replaced [11]. This could be done by a control unit placed outside the chamber. The debris was also prevented from moving too far in the chamber by keeping the pressure around 10 mbar. The sputtered particles collide with the air molecules and lose kinetic energy. The particular pressure is a compromise between keeping it sufficiently low to get as little distortion as possible in the laser focus and keeping it high enough to prevent the particles to hit the optics [11, 19].

The laser is a ten-hertz system at the High Power Laser Facility in Lund. The system was obtained in 1992 and has since then been continously upgraded. The system has two arms with different pulse energy at present. These arms can be used in different experiments at the same time. The arm used in this project can produce ~ 2 TW with a pulse length of ~ 35 fs and an average pulse energy of ~ 80 mJ/pulse.

The samples that were investigated were Si wafers, purchased from Compart Technology Ltd. Wafers of both 55 μm and 10 μm thicknesses were used, but no results were achieved with the 10 μm wafers. Bragg diffraction from InSb was also studied for reference and to check the aligning method, since the InSb crystals were easier to handle.

3.3 The CCD camera

The detector used in the experiments was a *charge coupled device* (CCD) camera, especially designed for detecting energies in the range 0.5-8 keV, i.e. the region for *soft X-rays*. The CCD was purchased from Princeton Instruments in the mid 90's. The CCD chip consists of 512×512 small picture elements, *pixels*. These are all individual semiconductor detectors that can be used simultaneousely to register photon energies.

3.3.1 The chip

The chip is made of thin crystalline silicon in a high-purity form. A thinner layer of silicon dioxide is put on one side, and on top of that there is a layer of *gate structure.* The gates are a kind of electrodes.

The size of the chip is 12.7×12.7 mm and it is divided into 512×512 pixels of size 24.8×24.8 μm. In front of the chip there is a beryllium window, 250 μm thick, which transmits the x-ray photons but prevents e.g. laser light to damage the chip. The chip is mounted approximately 10 mm behind the window inside a protective casing.

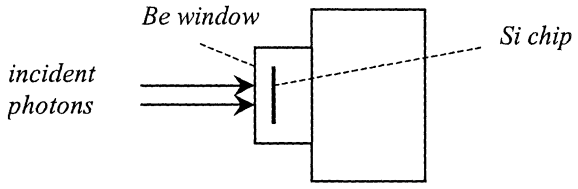

Figure 3.2. Schematic picture of the CCD camera.

The CCD chip is *back-illuminated* and *back-thinned.* The opposite, a *front-illuminated* chip, means that light first passes through the polysilicon gate structure before detection in the depletion area. The gates are almost opaque at wavelengths shorter than 400 nm, i.e. higher photon energies are considerably attenuated. Therefore a front-illuminated CCD is no good for detecting soft x-rays which are of a wavelength of the order 10^{-2}-10^{-1} nm. When the light is coming from the other direction (*back-illuminated*) the photons are incident directly on the pure silicon and the chip becomes more sensitive to shorter wavelentghs. The back side of the chip is also uniformly thinned to roughly 10 μm. Shorter wavelengths in the region of soft x-rays do not penetrate that deep into the chip so this method enhances the detection of higher energies.

3.3.2 Environment

The detector must be cooled to get a reasonable signal-to-noise rate, otherwise the thermal noise will be too much of a disturbance. The cooling is performed by a Peltier-element. Condensation inside the camera could cause interference with the optical signal or con-

tamine the instrument. To prevent this it must also be evacuated. A pressure of around 10 mbar is recommended from the manufacturer.

3.3.3 Principles

When photons hit the CCD chip they deposit their energy and electrons in the silicon are excited and electron/hole pairs are created. The direct bandgap in silicon is 1.1 eV, but for an electron/hole pair to be created a greater amount of energy is required. This amount is inversely proportional to the temperature [20].

The deposited photon energy may be used for two different processes; phonon production and ionisation [20]. The lattice excitation requires less energy than the ionisation, and many modes are possible. For every incident photon the deposited energy produces N_x phonons and N_i electron/hole pairs. The total energy E_0 is thus;

$$E_0 = N_x E_x + N_i E_i$$

The number of ionisations from each photon is:

$$N_i = \frac{E_0}{\varepsilon_i}$$

Here ε_i is the average energy required to produce an electron/hole pair. For silicon in the CCD the energy ε_i is about 3.65 eV.

The electrons are captured on electrodes and then transferred to an amplifier where the charge is converted to a voltage output signal. Further amplification takes place and eventually the signal is digitized in the analog-to-digital-converter (A/D) and sent to the connected computer where the image can be displayed and analyzed. The signal is thus direct proportional to the photon energy.

The CCD detects the photons and shows the result as a number of *AD-units* (ADU). For the CCD used in this project every freed electron corresponds to 3.65 eV. To recieve one ADU from the A/D-converter, there must be a specific quantity of electrons, referred to as the *gain* of the detector. The gain expresses the number of electrons per ADU. For the specific camera used here the gain is approximately 5.49 e^-/ADU. By multiplying the number of ADU with 3.65 and the gain 5.49 the signal is received in eV-units. The smallest energy unit of the detector is then approximately 20 eV.

X-ray photons have energies that would free 100-10000 electrons each. Since the background noise is much lower than one such signal, CCDs can be utilized for photon counting when detecting x-rays.

3.3.4 Background

There is always a *dark current* noise in the CCD. This background arises from thermal energy in the chip which creates electron/hole pairs. The noise follows Poisson statistics and it scales as the square root of the number of thermal electrons produced. By cooling the camera, as mentioned above, the dark current is reduced.

During the quantifying process an additional source of noise is added, the read noise. Most of it comes from one of the amplifier. Variations in the photon flux is also interpreted as noise. Poisson statistics holds for this noise too, and it is thus scaled as the square root of the signal.

3.3.5 Photon counting

When dealing with photon counting one would like to assume that the ADU number detected in each pixel correspond to *one* single photon event, but one cannot be completely sure of that. First there is the *pile-up problem*. If the exposure time is long enough two different photons may hit the same pixel and the pixel registers the accumulated value of their energies. Then there is the *smearing problem*. When a photon hits the detector it can deposit its energy in more than one pixel. The detector incorrectly registers more than one event and at lower energies than the actual value.

To avoid the problem with pile-up effects, one way to collect the information is to accumulate a number of pictures with relatively short exposure time and integrate them after proper processing with a summation algorithm. The software makes it possible to store all pictures in the same file and only one accumulation set-up and execution is made.

The smearing problem can be reduced by summing adjacent pixels together with a special algorithm in the image processing. Most common is the 3×3-pixel summation [21]. A photon event is recognised and the surronding 8 pixels are assumed to belong to the very same photon. Here, a special routine was written and it will be discussed in section 4.

We also need to take the read-out process into consideration. The CCD has an output node in the chip. It is a kind of read-out pixel. Data from all other pixels has to pass through this specific node to be registered. The read-out is made by a series of serial and parallel shifts. The data are first shifted in the serial (horizontal) direction into the serial register. When the row is in the register it is further shifted into the parallel (vertical) direction towards the output node and from there the A/D converting takes place. This process takes a certain time, about a second. If photons were allowed to hit the detector during the read-out they would appear on the screen as a kind of smeared pattern. This problem can be avoided mechanically:

A separate shutter can be connected to the CCD camera. It automatically closes when the read-out is performed and opens again when the next image is to be sampled. In this way additionally pile-up effects are prevented. For this particular experiment set-up there are however two problems with this item: The shutter is too small to stop the laser beam in front of the focusing lens and it would be damaged by the laser pulse if mounted after the lens. Therefore a special shutter set-up was constructed (*figure 3.3*).

Shutter set-up
The TW laser is also applied with a shutter that stops the laser beam. It can be controlled by a remote control box in the lab room. The special set-up was made to control the shutter at the TW laser with the camera shutter. A He-Ne laser was directed at a photodiode with the camera shutter in between. A 3 V voltage was applied and finally the remote control was connected to this circuit. When the camera shutter is closed the current is switched off and the shutter at the TW laser is also closed and thus no x-ray photons are produced during the read-out time.

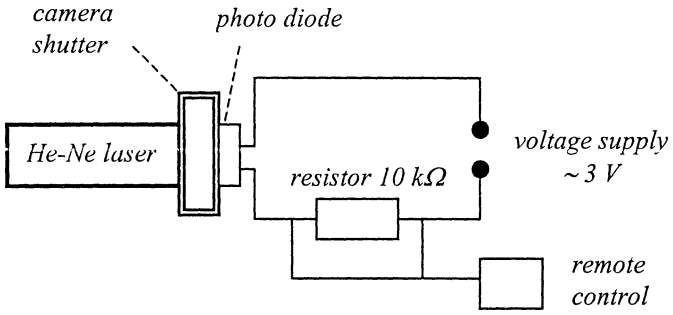

Figure 3.3. The shutter control set-up.

3.4 Optimising the lens

3.4.1 Set-up

When optimising the focus of the lens, the camera was placed just in front of the plastic window to detect as many photons as possible, *see figure 3.4*. The distance between the x-ray source and the CCD chip was 27 mm. The solid angle of the photon emission hitting the camera was 0.2 sr. The pressure in the vacuum chamber was set to 10 mbar. Both copper foil (50 μm) and molybdenum foil (150 μm) were investigated as targets.

The lens was set at ~ 300 mm from the target. When optimising the focus, the lens position was varied relatively by 1 mm for the Cu foil and 0.5 mm for the Mo foil. Respectively, a total distance of 10 mm and 4 mm was evaluated. At each lens position ten shots were performed and evaluated. Furthermore each position was set three separate times, i.e. a total of 30 shots were made at each measure point. The K_α photons were counted within a region ± 0.15 keV.

When testing the Mo target, the end position of the lens was reached in one direction. In the other direction the x-ray production went down below the measurable limit. The distance that could be analysed was divided into steps by 0.5 mm. The stationary translation stage was not moved for further investigation, since it was decided that the total number of photons in any case was too low to be of interest for the experiment.

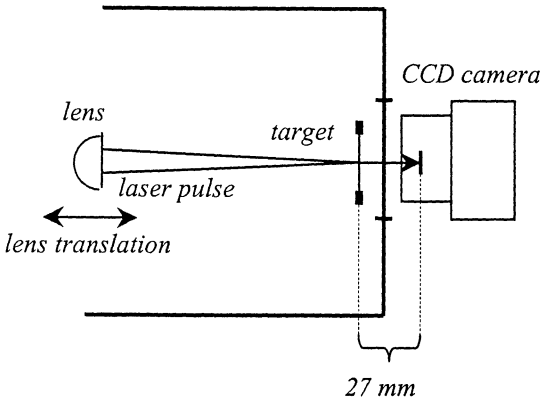

Figure 3.4. The set-up for measuring the x-ray generation during optimisation of the lens focus.

3.4.2 Result of lens optimisation

The copper target showed a significant relation between the lens focus position and the X-ray emission (*figure 3.5*).

The laser intensity was the same for the Cu target and the Mo target but the number of photons generated was considerably lower from the Mo target (*figure 3.6*). It is more difficult in general to generate harder x-rays, i.e. radiation from elements with higher Z number [10, 17, 18]. The foil was also thick and quite buckled, and not as smooth as preferred. This could have an effect on the x-ray generation since the focus position on the target then is not very well defined [11].

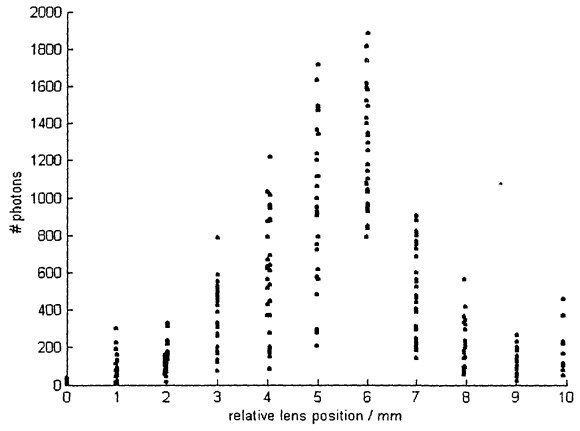

Figure 3.5. Photons counted at one single shots on Cu target for different lens positions.

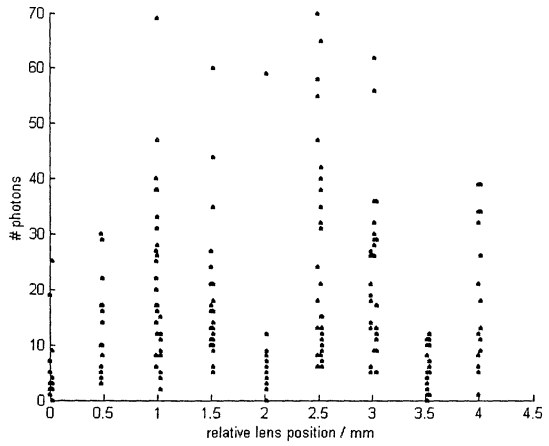

Figure 3.6. Photons counted for one single shots on Mo target for different lens positions.

3.5 Sample set-up

The Cu K_α photons have a wavelength of λ = 1.54 Å and the Si crystal has a lattice constant of a = 5.43 Å. The Bragg conditions for Si is fulfilled when $(h+k+l)$ equals a multiple of 4 or when all indices are odd (*see section 2.2.4-5)*. The Bragg angles for some lattice planes in Si are seen in *table 3.1*. The Bragg angles for Mo radiation are included for comparison.

Table 3.1. Bragg diffraction angles for λ =1.54 Å and λ=0.71 Å in Si crystals.

(hkl)	*θ_B [°] λ=1.54 Å (Cu K_α)*	*θ_B [°] λ=0.71 Å (Mo K_α)*
(111)	*14.2*	*6.5*
(220)	*23.6*	*10.6*
(311)	*28.0*	*12.5*
(400)	*34.6*	*15.2*
(331)	*38.2*	*16.6*
(422)	*44.0*	*17.0*
(333)	*47.5*	*19.9*

The deflection from the incident beam is twice the Bragg angle (*cf. figure 3.7*). Since the chip is small and the Bragg angles large it is not possible to detect more than one spot at the same time, since they would be to wide apart. Remember also that the sample cannot get any closer to the chip than 10 mm. This is why Mo radiation would be interesting, the diffractions angles are less than half of the angles for Cu. To be sure of detecting Bragg reflection, the wafer and the detector were carefully aligned, according to the aquired conditions.

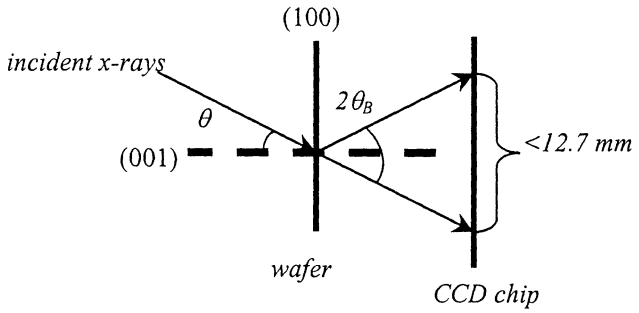

Figure 3.7. Laue diffraction from the (001) plane. The surface of the crystal is parallel to (100). The deflection from the primary beam, incident from the left, is $2\theta_B$. The size of the CCD chip is 12.7×12.7 mm.

The wafers have the surface orientation of (100). The easiest plane to align of the allowed ones is then the (400) plane, since it is parallel to the surface of the wafer. The Bragg angle is 34.6°. The wafer was oriented in the (100) direction, placed vertically on a rotational stage and aligned in the Bragg angle, relative to the direction of the x-ray fan that was set as 'zeroth' direction (*cf. figure 3.8*). The CCD camera was aligned behind the wafer so that it would catch the Bragg reflection. The idea was that when a Bragg (400) reflection was detected, the crystal should be turned 90° for Laue transmission reflection from the plane perpendicular to the (400) plane (*cf. figure 3.7*). The x-ray beam was not collimated and the detector was screened from the x-rays by a lead block so that only the diffracted photons would reach the chip.

To ensure the reliability of the set-up and the Si wafers, a more rigid crystal was tested first. A sample of InSb - a = 6.47 Å, θ_B = 11.9° for Cu K_α and (111) - was studied. Bragg diffraction from this crystal was aquired with the set-up seen in *figure 3.8.* Laue transmission pattern was not possible though, since the crystal was too thick for transmitting sufficient number of photons.

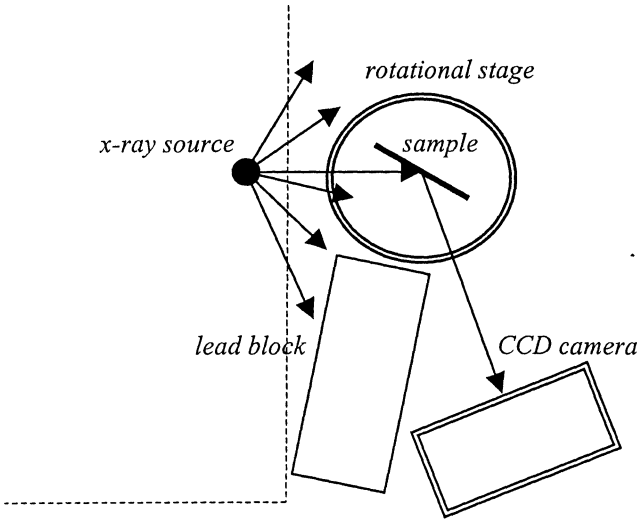

Figure 3.8. The geometry for Bragg reflection. The distance from the source to the sample is about 5 cm and the distance from the sample to the CCD is about 10 cm.

3.5.1 Diffraction results

To be able to see the Bragg reflection directly in the lab, one long exposure of 60 seconds was made. The summation algorithm could not be performed directly, since the image processing was done on another computer not located in the lab room. In images taken at shorter exposures than 30 seconds it was difficult to recognise the Bragg reflection directly.

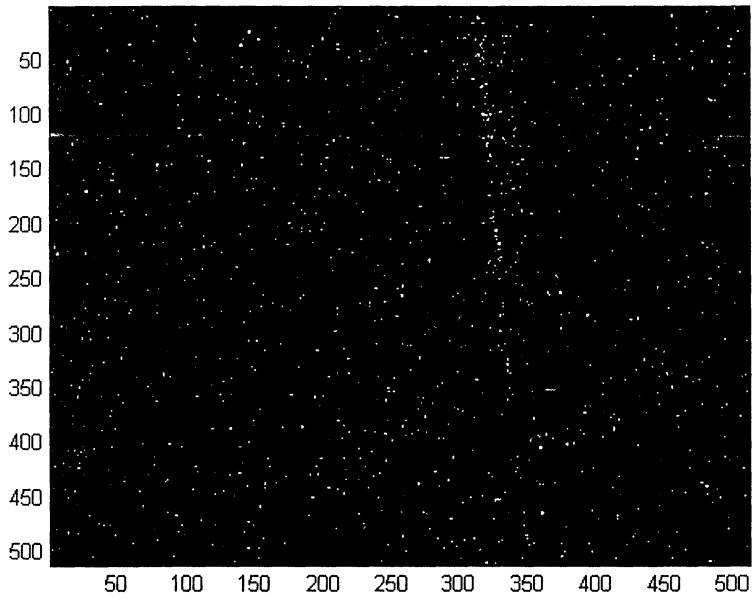

Figure 3.9. Bragg reflection from Si (400). The width of the reflection is approximately 0.02 rad. The exposure time is 60 seconds.

3.6 Experimental problems

There were some difficulties with the assignment and not many results were achieved. Only a few pictures with Bragg diffraction were accomplished. There are two main difficulties, which prevented further progress within the limited time frame:

The accuracy in the wafer mounting is extremely important. To find the Laue reflection from the Bragg reflection, the wafer has to be mounted exactly on the rotational axis from the rotational stage so that the correct angle is set. The Bragg spot (*figure 3.9*) was estimated to have a width of 0.02 rad. When rotating the sample 90° from the Bragg position the error from the rotation was larger than the width and the alignment was lost. The situation was similar to the needle in the haystack.

The surface of the crystal is also very bendy. If the wafer is buckled the planes are no longer plane and the Bragg reflections cannot be seen. This is a major problem, especially with the thinnest wafers (10 μm). Several attempts were made but none gave a satisfactory result. They were too soft and sensitive for buckles that no Bragg diffraction was possible.

The 55 μm wafers did show Bragg reflection (*figure 3.9*) but no Laue spot was detected. The transmission for 8 keV (Cu K_α) in 55 μm Si, is only 0.45 [22]. This makes it of course harder to detect Laue spots. With a weaker signal the exposure time must be longer and then more scattered x-rays are registered on the chip.

3.6.1 Additional attempts

Before the final set-up was tested some other attempts were made. The problem was to catch more than one reflection on the detector. First of all the goal was to detect a Laue spot on the CCD. From the beginnig of this experiment a pinhole was used which made the x-ray beam divergent by an angle of approximately 0.01 rad (*figure 3.10 a)*). The sample and the camera were aligned according to the Bragg conditions for the plane perpendicular to the surface of the wafer; (040). The attempt did not give any diffraction pattern.

This divergence from the pinhole and hence, the intensity of the radiation was not considered sufficient. Therefore the pinhole was changed into a plastic window where a large divergence was achieved. In order at least to have the 'central spot', i.e. a non-diffracted beam, as a reference spot, the set-up in *figure 3.10 b)* was tested. The divergence was limited by lead shields mounted in front of the wafer. The central spot was detected straight in front of the source. A Laue spot from the (040) plane was intended to appear on the CCD after moving the camera in the lateral direction. The translation of the camera would correspond to the required Bragg angle. This set-up gave no results, probably because the incident angle didn't match the Bragg angle and/or the central spot and the Laue spot could not simultaneously be caught on the chip (*cf. figure 3.7)*.

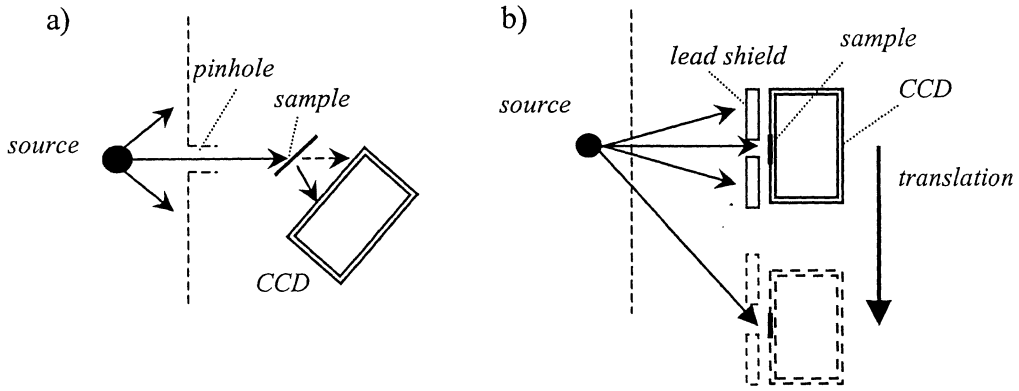

Figure 3.10. Experimental attempts to detect Laue spots from 55 μm Si wafers. a) *The x-ray beam has a small divergence through the pinhole; the size is exaggerated in the figure.* b) *The sample is mounted on the CCD and the divergence of the x-rays is restricted by lead shields.*

4 Image processing

The CCD chip consists of 512 x 512 pixels. Each pixel registers an integer number, which corresponds to the deposited energy in the pixel. The CCD software saves these values as a 512 x 512 matrix, in one image file, which can be analysed and displayed in the very same program if preferred, but it can also be processed in other programmes. The CCD software makes it possible to save a series of successive exposures in the same file. This make the experimental procedure more easy when trying to optimise the signal-to-noise ratio (SNR) and minimise the pile-up effects, i.e. when two photons hit the same pixel. The execution button is pressed only once but several images are taken. Processing each exposure and then integrating the results afterwards should give a better result than one single exposure of the same length as the total time of the shorter exposures. For this project the images was processed in Matlab 6.1. The program code is shown in the Appendix. An example of an x-ray image is shown in *figure 4.1.*

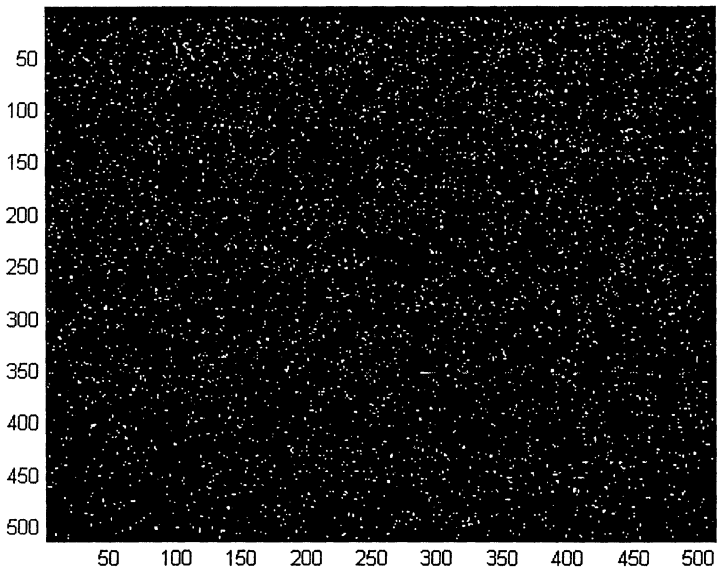

Figure 4.1. Image after one single shot on Cu target, background subtracted. The set-up is the same as shown in figure 3.4.

The first task was to view the energy spectrum of the CCD image (*figure 4.1*). This was made by photon counting where every pixel was treated as one single photon event. A histogram was made with a binning of 60 eV. This resolution was considered sufficient since we are interested in the K_α- and K_β-peaks, which were found to have a width of about 0.2 keV. The background pixels (~3.5 keV) dominates the pictures and the peak is about 100-1000 times stronger than the K_α- and K_β-peaks (*figure 4.2*). One way to get rid of the background is of course to take a non-exposed image with background only and then subtract it from the x-ray image. However, the background varies, both in different exposures and spatially within the picture. The variation is approximately 0.1 keV. The attempt was to evaluate the local background to avoid the effect of exposural and spatial differences.

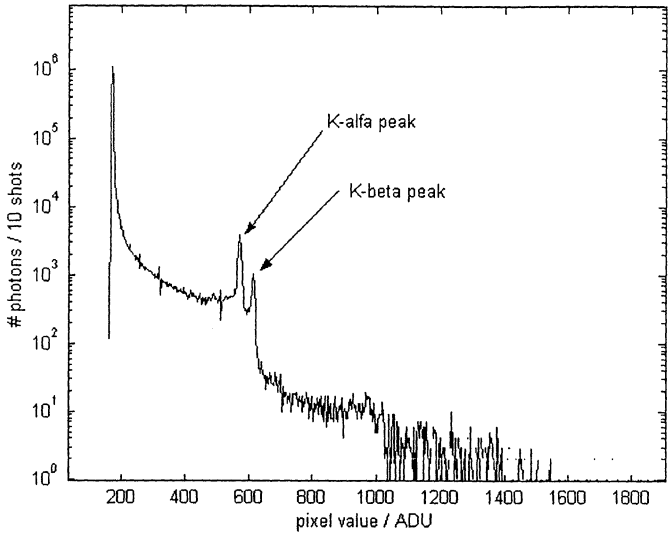

Figure 4.2. Photon counting including background, Cu target.

4.1 Background subtraction

The interesting pixels are those that with a value higher than the background. In a first approximation the background level is set to a plausible value by just looking at the background peak in the raw histogram. The program finds the pixels that are higher than this value and then looks closer to the eight nearest neighbours. The mean value of those neighbouring pixels that are lower than the approximate background is subtracted from the central pixel. In the rare cases where there are no background neighbours the approximate value is used. All pixels identified as background pixel are set to zero.

4.2 Summation of adjacent pixel events

It can happen that a photon deposits its energy in more than one pixel. The energy could be smeared out over several adjacent pixels according to the image in *figure 4.3* and the matrix part in *figure 4.4*. To count these events as one single photon the pixels are often summed together. Most commonly the pixels are summed 3×3 around a central pixel event. The central pixel is the brightest pixel in the neighbouring area and identified as a 'main' photon event and the adjacent pixels are assumed to originate from the same event. But it is not possible to know that this is the correct method; the energy might for instance be unequally spread around the main pixel, or the main pixel is perhaps not the brightest one [21].

In this project an additional algorithm was written, with another approach than 3×3 summation. When looking closer to the matrix it seemed reasonable to add pixels together according to a specific pattern. Eight different modes were chosen, including the one single pixel mode (*figure 4.5*). After subtracting the background the program searches for structures like these templates. If such a template is found, the pixels included are assumed to originate from the same photon and the sum of them will be counted as one single photon event.

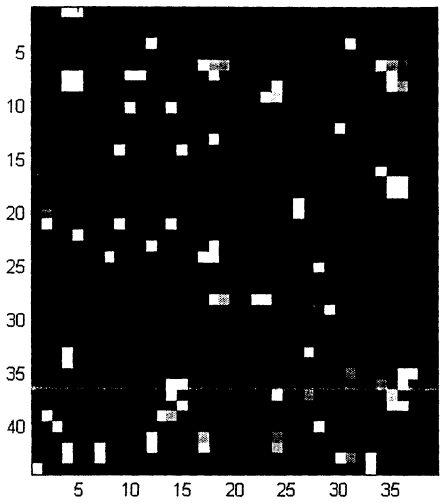

Figure 4.3. Enlarged part of a one-shot image.

65	0	0	396	0	0	90	11	0	0	0	325	12	0	0	0	0
23	0	0	0	0	0	43	215	153	0	398	0	360	0	0	0	0
159	29	0	0	130	51	0	0	0	0	0	0	0	419	0	0	0
396	0	0	0	0	0	0	0	0	0	0	0	0	0	0	0	0
0	0	0	0	0	0	0	0	406	0	0	0	0	74	225	0	0
0	0	0	0	0	0	0	417	0	0	0	0	0	0	0	38	348
0	0	0	0	0	0	0	295	0	0	0	0	0	0	0	0	0
0	151	620	0	0	0	0	0	47	14	0	0	0	0	0	0	0
0	0	0	0	0	0	0	0	226	49	0	0	0	0	0	0	29
0	0	0	0	0	0	0	0	0	0	0	0	0	0	0	0	279
0	0	0	0	0	30	0	0	0	0	0	0	0	0	0	0	0
17	13	0	0	0	94	0	0	0	0	0	0	0	0	0	110	0
41	44	0	0	144	0	0	0	0	0	0	0	0	0	0	35	0
0	0	0	0	0	0	0	0	0	45	203	0	0	0	49	119	0
0	0	0	0	0	0	0	0	0	83	93	0	0	0	0	366	0
0	0	0	0	0	0	425	0	0	29	27	0	0	0	0	0	99
0	0	0	0	0	0	0	0	0	0	0	0	0	0	0	0	0
0	37	0	0	0	0	0	0	0	0	0	0	0	0	0	0	0
0	0	0	0	0	0	0	0	0	0	0	16	0	0	0	0	0
0	0	0	0	0	0	0	0	0	0	0	0	0	0	0	0	0
0	0	0	276	0	0	0	0	0	0	0	0	0	450	15	358	0
24	0	0	33	0	0	0	0	0	0	394	0	0	0	0	0	0

Figure 4.4. Part of an image 512x512 matrix. The background is here subtracted. Events that would be counted in the summation algorithm are shadowed.

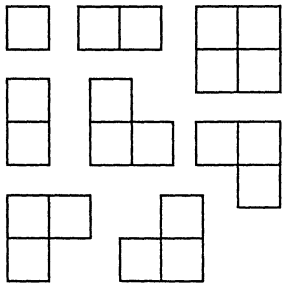

Figure 4.5. Templates for photon events.

If there are more than four adjacent photon events, or if they are not grouped like one of the presented templates, the probability that the pixel group belongs to more than one single photon increases. The difficulty is then to decide how to sum the pixels, but that is beyond the scope of this work, so the treatment of those 'clusters' is simply to ignore them.

The cross section for Compton scattering for 8 keV in Si (CCD chip) is considered negligable in this context and is therefore not included in the process. At higher x-ray energies this effect is of greater importance [19].

This algorithm works best with short exposures where the photons are few and don't lie too close.

4.2.1 Result of pixel event summation

The photon counting for Cu and Mo targets, before summations are shown in *figure 4.6* and *4.8*. The shapes of the curves corresponds to the theory discussed in section 2.3; the Brehmsstralung emission is proportional to the Boltzmann distribution, $exp(-E/kT_e)$ [14].

The results of the summations for Cu and Mo targets are shown in *figure 4.7* and *figure 4.9* respectively. The peaks of the K_α and the K_β photons for Cu target are somewhat lower after the summation of the smeared-out photons (*figure 4.6* and *4.7*). This may be due to the fact that photons have been discarded when they are to close to one another, e.g. a gathering of more than four adjacent events. The small peak at 6.40 keV could possibly originate from characteristic radiation from Fe in the target holder.

The x-ray generation from the Mo target was not as successful as with the Cu target. The number of photons is considerably lower. This was expected, since the x-ray yield is lower from targets with higher Z number [10, 17, 18]. The probabilities for pile-up effects and for two photons to hit neighbouring pixels are lower. The result of the summation shows that more K_α photons are counted with the summation algorithm. This supports the idea that the algorithm works better for images that are more sparsely populated.

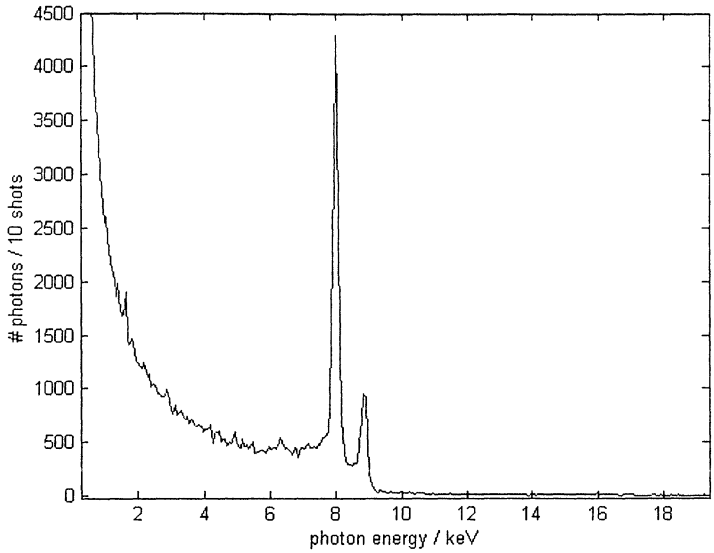

Figure 4.6. Number of photons for ten shots on Cu target, background subtracted.

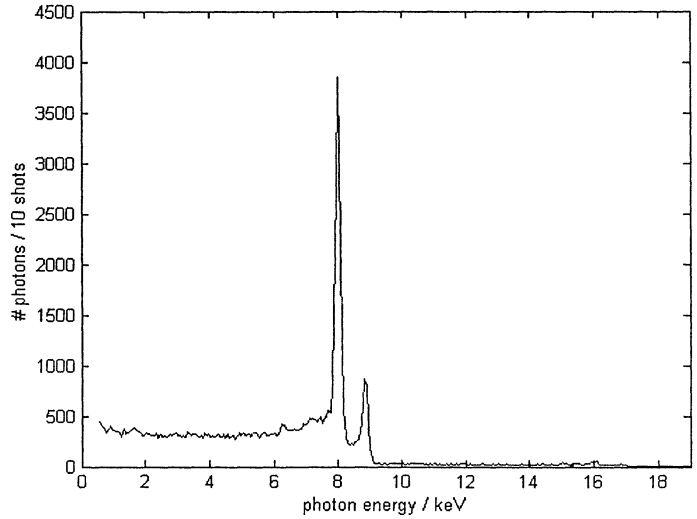

Figure 4.7. Photons counted for ten shots on Cu target after processing the images with the summation algorithm.

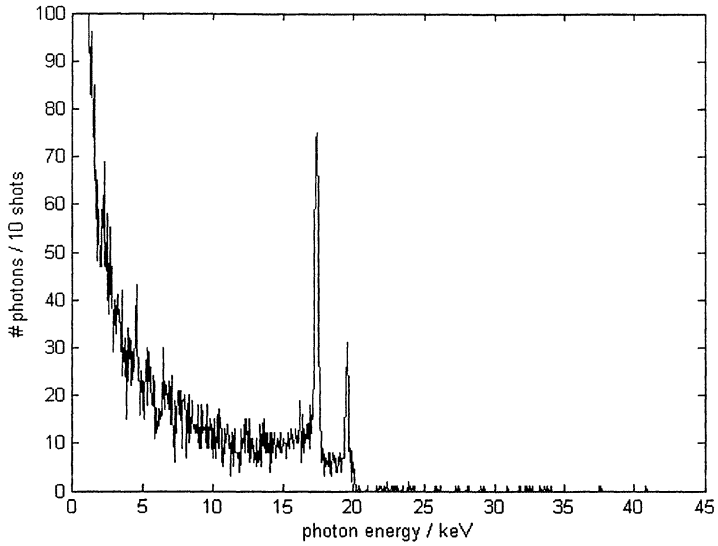

Figure 4.8. Photons counted for ten shots on Mo target, background subtracted.

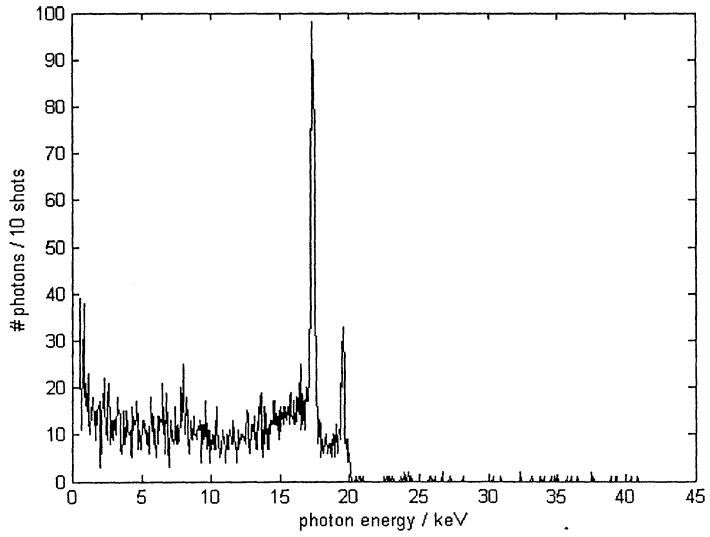

Figure 4.9. Photons counted for ten shots on Mo target, after processing the images with the summation algorithm.

4.3 Energy selection

By selecting a specific energy interval the scattered photons in the images can be reduced. Of course this is useful when looking at x-ray diffraction, since the only interesting photons are those that are scattered elastically. *Figure 4.10* shows Bragg reflection from InSb (111). There are different exposures of totally 120 seconds added together, showing all energies from 0 to ~20 keV. The broader line to the left in the pictures is due to scattered photons that were not blocked by the lead block.

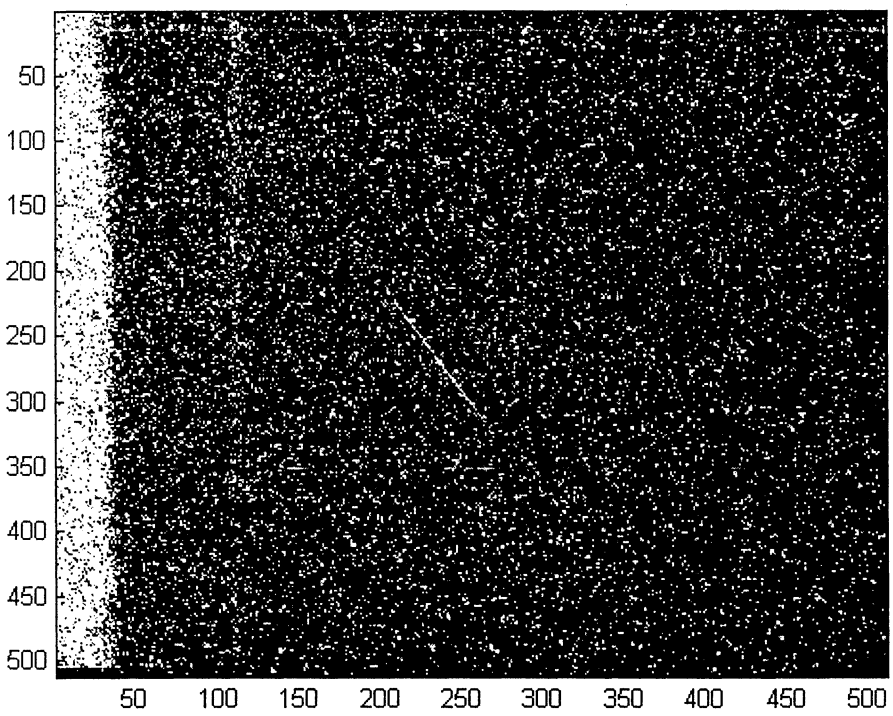

Figure 4.10. Bragg diffraction from InSb (111). The image shows photon energies 0-20 keV, approximately.

For exposures of this order the diffraction line is still clear, but it could perhaps be a problem if the total exposure time was longer. Weaker Bragg spots could be concealed in the image when inelasticcally photons dominate the screen. The image should be compared to *figures 4.11-12*, which show photons only in the interval 7.85-8.15 keV (~ Cu K_α). At this short exposure time, the diffraction spot is more clearly visible if all energies are shown. But still, it could be useful to get rid of all scattered background photons. For longer exposures these scattered photons are too dominating and the energy selecting procedure is more useable.

The difference between addition of non-processed images and pixel-summed images can be seen in *figures 4.11-12*. Even shorter time for each exposure might improve the result since there would be fewer photons in each exposure and the discarding of events that are too large (more than four adjacent events) would decrease.

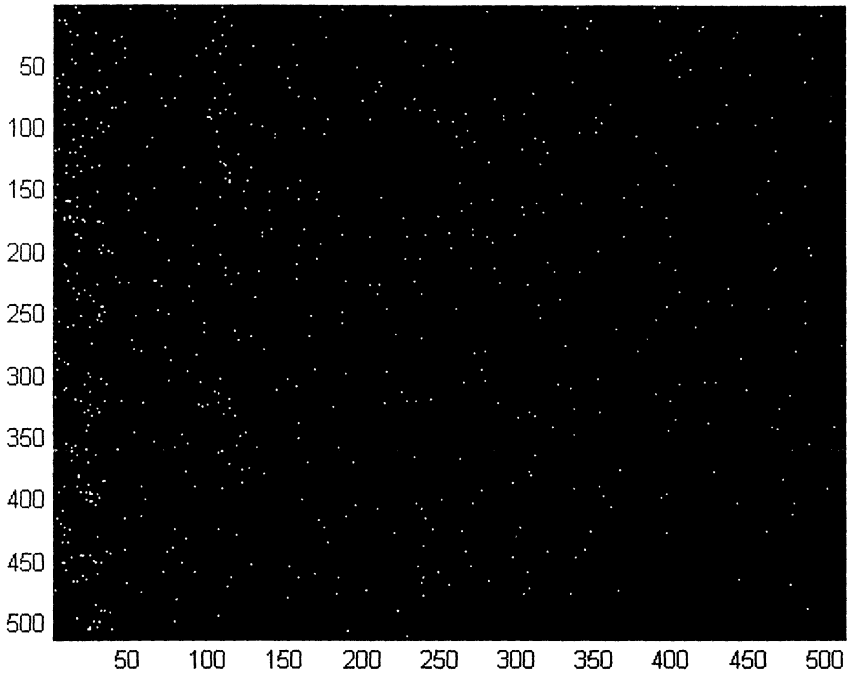

Figure 4.11. Image of Bragg reflection from InSb (111). The image is the result of adding several exposures to a total of 120 seconds. The image contains only photons of energies 7.85-8.15 keV.

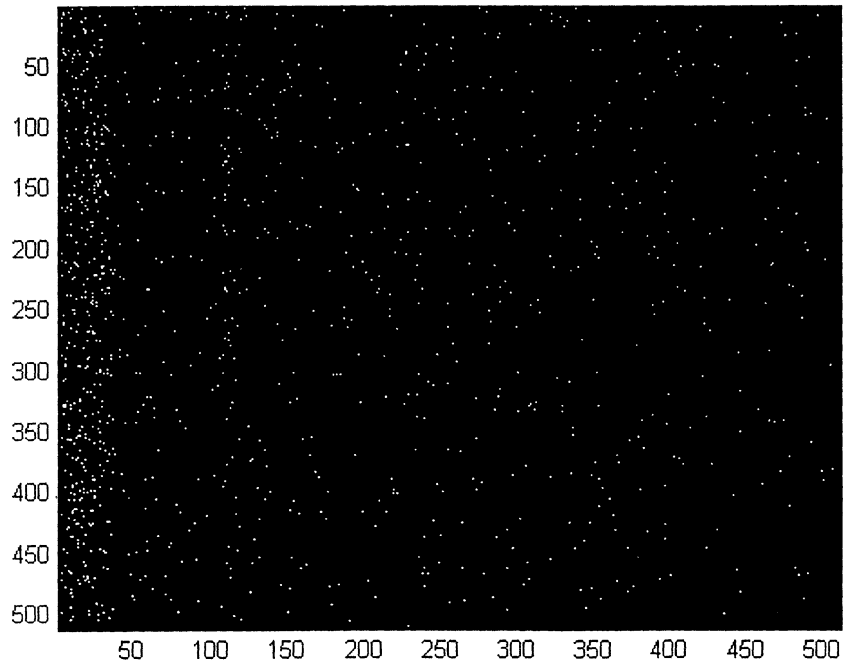

Figure 4.12. Image of Bragg reflection from InSb (111). The image is the result of adding several exposures to a total of 120 seconds, after processing each of them with the pixel-summation algorithm. The image contains only photons of energies 7.85-8.15 keV.

5 Summary

This diploma work was a study of a new geometry for ultra-fast time-resolved diffraction experiments. The aim was to develop a working set-up for further pump-probe studies. Thin silicon wafers were used as samples and the laser-produced plasma as x-ray source. The idea was that by using a monochromatic but divergent source, several Bragg reflections would be detected simultaneously and the accumulation time for such experiments would decrease.

The main parts were devoted to the evaluation of the experimental set-up and to image processing of the data output.

5.1 Part one: Experimental set-up

The set-up evaluated in this project was supposed to be a compact and easy-to-use set-up. The pump and the probe beam could easily be synchronised by linking the pump beam from the pulsed laser, which creates the probe pulse. The pulse-to-pulse fluctuations would play an insignificant part and the experimental set-up would be less sensitive for this kind of variation.

The experimental set-up work did not progress as intended, due to technical diffficulties. The result of this thesis part has mainly been the excluding of some non-usable set-ups. However, I do think it is possible to achieve a user-friendly experimental geometry. For instance, a little more engineering work is required to complete the sample holder. That was not given priority in this project, due to the time limit. Maybe some kind of frame that straightens the wafer, without blocking the x-rays would help, or perhaps the wafer could be mounted on a thin plate of a suitable material, which transmits a sufficient part of the radiation. In this project no special frame was invented or manufactured.

5.2 Part two: Image processing

The main result of the diploma project was the image processing. The pixel summation algorithm showed satisfactory results. More events were detected by summing adjacent pixel if the exposures didn't contain too many pixel signals. When two events are lying too close the algortihm ignores them. That is probably what happened to the test images with Cu K_α, analysed in section 4.2, where the summation algorithm decreased the number of detected K_α-photons. However, when a 'real' experiment is performed the photons of interest will not be that close if the exposure time is sufficiently short.

The program is easily extended for other conditions, e.g. events spread on larger area than 2×2 pixels. The experimental performance regarding the exposure time must be adjusted to the imaging process. The shorter exposures the better result with the program.

The energy selective process also showed great results. Unfortunately, no total exposure time longer than 120 seconds was performed but one could still see the improvement in the current images. The inelastically scattered, non-diffracted photons are thereby disposed. This will make the intended image more visually clear.

6 Acknowledgements

First of all I would like to thank my supervisor, Jörgen Larsson, who has been a great support during all this time. He has shown great patience and explained both trivial and advanced matter to me. He has believed in me and given me responsibilities in the lab, which have made me learn a lot.

I'm also very grateful for the help I got from Anders Persson with the TW laser.

Thanks to Ola Synnergren for helping me with computers, cables and answering questions, to Michael Harbst for helping me with equipment and back-up copies on his computer and to Tue Hansen for answering questions and being a great room-mate.

Finally, thank you all who have shown interest in my work, and all who have helped me with this project in some way or another.

Thanks!

7 Bibliography

[1] A. M. Lindenberg, I. Kang, S. L. Johnson, T. Missalla, P. A. Heinmann, Z. Chang, J. Larsson, P. H. Bucksbaum, H. C. Kapteyn, H. A. Padmore, R. W. Lee, J. S. Wark and R. W. Falcone, *Phys. Rev. Lett.* **84**, 111 (2000)

[2] V. Srajer, T. Teng, T. Ursby, C. Pradervand, Z. Ren, S. Adachi, W. Schildkamp, D. Bourgeois, M. Wulff and K. Moffat, *Science* **274**, 1726 (1996)

[3] C. W. Siders, A. Cavalleri, K. Sokolowski-Tinten, Cs. Toth, T. Guo, M. Kammler, M. Horn v. Hoegen, K. R. Wilson, D. v. der Linde and C. P. J. Barty, *Science* **286**, 1340 (1999)

[4] A. Rousse, C. Rischel and J-C. Gauthier, *Rev. Mod. Phys.* **73**, 17 (2001)

[5] J. Larsson, *Opt Lett.* **26**, 295 (2001)

[6] J. D. Stephenson, *Appl. Surf. Sci.* **96-98**, 528 (1996)

[7] J. Larsson, P. A. Heimann, A. M. Lindenberg, P. J. Schuck, P. H. Bucksbaum, R. W. Lee, H. A. Padmore, J. S. Wark and R. W. Falcone, *Appl. Phys. A.* **66**, 587 (1998)

[8] T. d'Almeida, M. Di Michiel, M. Kaiser, T. Buslaps and A. Fanget, *J. Appl. Phys.* **92**, 1715 (2002)

[9] J. Larsson, A. Allen, P. H. Bucksbaum, R. W. Falcone, A. Lindenberg, G. Naylor, T. Missalla, D. A. Reis, K. Scheidt, A. Sjögren, P. Sondhauss, M. Wulff and J. S. Wark, *Appl. Phys. A.* **75**, 467 (2002)

[10] A. Rousse, P. Audebert, J. P. Geindre, F. Falliès, J. C. Gauthier, A. Mysyrowicz, G. Grillon and A. Antonetti, *Phys. Rev. E.* **50**, 2200 (1994)

[11] M. Grätz, PhD Thesis, *Lund Reports on Atomic Physics, LRAP – 236*, (1998)

[12] A. Rousse, C. Rischel, S. Fourmaux, I. Uschmann, S. Sebben, G. Grillon, PH. Balcou, E. Förster, J.P. Geindre, P. Audebert, J. C. Gauthier and D. Hulin, *Nature* **410**, 65 (2001)

[13] A. H. Chin, R. W. Schonlein, T. E. Glover, P. Balling, W. P. Leemans and C. V. Shank, *Phys. Rev. Lett.* **83**, 336 (1999)

[14] C. Tillman, S. Å. Johansson, B. Erlandsson, M. Grätz, B. Hemdal, A. Almén, S. Mattson and S. Svanberg, *Nucl. Instrum. Methods* **394**, 387 (1997)

[15] D. Boschetto, C. Ricshel, I. Uschmann, J. Perez, S. Fourmaux, D. Hulin, E. Förster and A. Rousse, *J. Appl. Cryst.* **36**, 348 (2003)

[16] J. Larsson and A. Sjögren, *Rev. Sci. Instrum.* **70**, 2253 (1999)

[17] N. Uesugi, H. Nakano and T. Nishikawa, *CLEO, Pacific Rim '99*, 228 (1999)

[18] E. Andersson, G. Hölzer, E. Förster, M. Grätz, L. Kiernan, A. Sjögren and S. Svanberg, *J. Appl. Phys* **90**, 3048 (2001)

[19] A. Sjögren, PhD Thesis, *Lund Reports on Atomic Physics, LRAP – 288*, (2002)

[20] C. J. S. Damerell, *Rev. Sci. Instrum.* **69**, 1549 (1998)

[21] *Science Instrument (SI) Operations Handbook for the AXAF CCD Imaging Spectrometer (ACIS)*, version 2.65 (1997), http://www.astro.psu.edu/xray/docs/sop/, 2003-04-15

[22] http://www-cxro.lbl.gov/optical_constants/filter2.html, 2003-04-15

Appendix

Also available at: http://www-atom.fysik.lth.se/txrd/evaprog.m

Image processing code
Matlab 6.1.

```
% Initial values for some variables
count=512*512;
bild=0;bild2=0;bild3=zeros(512);
bildtot=0;bildtot2=0;bildtot3=0;
h(1:2000)=0;hh(1:2000)=0;hhh(1:2000)=0;
m=0;mm=0;mmm=0; c=0;

% Templates for summation of adjacent events
mat(:,:,1)=[1 0 1 1;0 1 0 1;1 0 1 1;1 1 1 1];mat(:,:,2)=[1 0 1 1;0 1 0 1;0 1 0 1;1 0 1 1];
mat(:,:,3)=[1 0 0 1 ;0 1 1 0 ;1 0 0 1;1 1 1 1];mat(:,:,4)=[1 0 1 1 ;0 1 0 1;0 1 1 0;1 0 0 1];
mat(:,:,5)=[1 0 0 1;0 1 1 0;0 1 0 1 ;1 0 1 1];mat(:,:,6)=[1 0 0 1;0 1 1 0;1 0 1 0;1 1 0 1];
mat(:,:,7)=[1 0 0 1; 0 1 1 0; 0 1 1 0;1 0 0 1];mat(:,:,8)=[1 1 0 1;1 0 1 0;0 1 1 0;1 0 0 1];

% File input
f=fopen('Si400.spe');
fread(f, 4100, 'uint8'); % The first 4100 bits are not image information

% To be able to integrate several images from the same file:
while count==512*512
        [i, count]=fread(f, [512 512], 'uint16');

   if count==512*512
      bild=i;
      clear a foton n x;
      a=max(max(bild));

      if a>m  % m is the maximum length of the x-axis
         m=a;
      end

      % Histogram:
      x=0:3:a;
      n=hist(bild,x);
      foton=sum(n');
      a=round(a/3);
      h(1:a-1)=h(1:a-1)+foton(1:a-1); % Add histograms
      bildtot=bildtot+bild; % Add images

      % Approximative background:
      bak=0;
      a=(max(bild));
      a=max(a);
      x=0:3:a;
      n=hist(bild,x);
      foton=sum(n');
      bak=find(foton==max(foton));  % Find background peak

      % Sort out pixels that are higher than background
```

```
mall=bild>(bak*3+8);
bild2=mall.*bild;
[u,v,varde]=find(bild2);

% Go through all identified photon events:
bild3(1:512,1:512)=0;
for k=1:(length(u))
   uu=u(k);vv=v(k);
   if uu==1 | vv==1 | uu==512 | vv==512
      bild2(uu,vv)=(bak*3+8); % Pixels on the edge are transformed to background
      medel=bak*3+8;
      p=0;
   else

  % Look at 8 nearest neighbours
   bildsort=(bild(uu-1:uu+1,vv-1:vv+1));
   % Sort values according to size
   bildvek=[bildsort(1,:) bildsort(2,:) bildsort(3,:)];
   s=sort(bildvek);
   p=find(s<bak*3+8);
   p=length(p);
   end %if-end

   if p>0
   medel=round(mean(s(1:p)));
   end % if-end

   % Background subtraction
   bild2(uu,vv)=bild2(uu,vv)-medel;

end % for-end

a=max(max(bild2));
if a>mm
  mm=a;
end

% Histogram #2
xx=0:3:a;
nn=hist(bild2,xx);
foton2=sum(nn');
a=round(a/3);
hh(1:a-1)=hh(1:a-1)+foton2(1:a-1);
bildtot2=bildtot2+bild2;

% Sum adjacent pixel events
   for j=1:length(u);
     uu=u(j);vv=v(j);

   if uu>1 & uu<511 & vv>2 & vv<511 % Events at the edge are discarded.
   if bild2(uu,vv-1)==0 & bild2(uu-1,vv)==0 % The events are only treated once
   pp=1; % Initital value for while-loop

       while pp<=8
          if pp<8
             if bild2(uu-1:uu+2,vv-1:vv+2).*mat(:,:,pp)==bild2(uu-1:uu+2,vv-1:vv+2)
                break
```

```
                end
            else
                if bild2(uu-1:uu+2,vv-2:vv+1).*mat(:,:,pp)==bild2(uu-1:uu+2,vv-1:vv+2)
                    break
                end
            end
            pp=pp+1;
        end

        if pp>1 & pp<8
            bilds=sum(bild2(uu:uu+1,vv:vv+1));
            bilds=sum(bilds');
            bild3(uu,vv)=bilds;

        elseif pp==8
            bilds=sum(sum(bild2(uu:uu+1,vv-1:vv)));
            bild3(uu,vv)=bilds;

       elseif pp==1
        bild3(uu,vv)=bild2(uu,vv);

       end
     end % if-end
     end % if-end
  end % for-end

    a=max(max(bild3));
    if a>mmm
    mmm=a;
    end

     % Histogram #3
     xxx=0:3:a;
     nnn=hist(bild3,xxx);
     foton3=sum(nnn');
     a=round(a/3);
     hhh(1:a-1)=hhh(1:a-1)+foton3(1:a-1);
     bildtot3=bildtot3+bild3;
     % Count images that have been processed
          c=c+1

 end % if-end
end % while-end

%Plot histograms

figure(1);
x=0:3:m;
plot(x(1:round(m/3)),h(1:round(m/3)));
semilogy(x(1:round(m/3)),h(1:round(m/3)));

figure(2);
xx=0:3:mm;
plot(xx(10:round(mm/3))*0.020038,hh(10:round(mm/3)));

figure(3);
xxx=0:3:mmm;
plot(xxx(10:round(mmm/3))*0.020038,hhh(10:round(mmm/3)));
```